Continuous-time quantum walk on an extended star graph: Disorder-enhanced trapping process

Saad Yalouz and Vincent Pouthier*
Institut UTINAM, Université de Franche-Comté, CNRS UMR 6213, 25030 Besançon Cedex, France

(Received 16 September 2019; published 28 January 2020)

Using a tight binding model, we investigate the dynamics of an exciton on a disordered extended star graph whose central site acts as an energy trap. When compared with what happens in an ordered network, our results reveal that the disorder drastically improves the excitonic absorption that becomes complete. Moreover, we show the occurrence of an optimal disorder for which the absorption time is strongly minimized, a surprising effect that originates in a disorder-induced restructuring process of the exciton eigenstates. Finally, we also show the existence of an optimal value of the absorption rate that reduces even more the absorption time. The resulting superoptimized trapping process is interpreted as a positive interplay between both the disorder and the so-called superradiance transition.

DOI: 10.1103/PhysRevE.101.012310

I. INTRODUCTION

Excitonic trapping is a key issue for explaining many phenomena in molecular lattices [1–5]. Examples among many are the time evolution of fluorescence processes [6] and excitonic transport efficiency [7], to cite but a few. Although most seminal works were initially devoted to translational invariant networks [8–10], recent studies have been realized to investigate excitonic trapping in more complex molecular networks. In this context, two kinds of systems have been considered simultaneously.

On the one hand, the excitonic trapping process has been studied in various realistic molecular networks including the Fenna-Matthews-Olson (FMO) complex [11] and polymer structures such as dendrimers [12]. The FMO complex, encountered in green sulfur bacteria, is a pigment-protein complex that involves seven bacteriochlorophyll-a molecules. In this protein, the capture of light generates excitons that converge toward a reaction center acting as an irreversible trap. On this specific site, the trapping of excitons initiates the photochemistry that ultimately leads to the chemical storage of energy [13–16]. Similarly, a dendrimer whose terminal groups are functionalized by chromophores can play the role of an artificial light-harvesting complex [17–22]. In this context, the absorption of photons by the chromophores generates excitons that propagate through the branches of the molecule to reach the core site, which contains either a fluorescent trap, a reaction center, or a chemical sensor [23,24].

On the other hand, from a more formal point of view, the excitonic trapping process has been studied in various complex networks including hyperbranched fractals [25], Sierpinsky fractals [26], cycle graphs with long-range interactions [27], chains and rings [28–30], and random networks [31]. These works, intimately connected to graph theory, exploit the formal resemblance between the excitonic delocalization occurring in nature and the concept of continuous time quantum walk (CTQW) [32]. As the quantum analog of classical random walk, CTQW has been extensively studied on complex networks during the past few years due to its various applications ranging from the research into perfect quantum transport [33] to the development of high-performance algorithms [34,35].

In that context, to judge the efficiency of the excitonic trapping process, the fundamental question arises whether the exciton delocalizes coherently or localizes along the networks. Although this problem still remains open, recent works suggest that the localized or delocalized nature of the exciton depends on important features such as the exciton-trap coupling strength, the network symmetry, and the presence of disorder [32].

First, the coupling with traps has a very pronounced impact on the efficiency of the excitonic propagation [36–38]. Resulting from the interaction with an external continuum, the trapping effect is usually taken into account using a non-Hermitian exciton Hamiltonian with complex eigenvalues. The real parts of these eigenvalues define the excitonic energies, whereas the imaginary parts specify the energy widths, i.e., the decay rates. In that case, a detailed study of these decay rates has revealed the occurrence of a general phenomenon called superradiance transition (ST) [39]. When the exciton is weakly coupled to traps on a network, all the excitonic eigenstates are similarly affected and exhibit quite similar decay rates. However, as the exciton-trap coupling increases, an eigenstate restructuring occurs. Only a few short-lived states, called superradiant states, exhibit cooperatively enhanced decay rates. These states are accompanied by subradiant eigenstates which represent long-lived states almost decoupled from the traps. As the exciton-trap coupling increases, the superradiant states strongly localize on the traps. As a result, the excitonic transfer to those specific sites is drastically hindered and the trapping process loses in efficiency.

Then, as shown by Mulken *et al.* [40], localization processes may also result from the degeneracy of the excitonic spectrum arising for networks with symmetries. In this case, when the excitonic quantum state initially expands over

*vincent.pouthier@univ-fcomte.fr

few highly degenerate eigenstates, specific quantum self-interferences arise. The propagation of the exciton is thus stopped, and the exciton remains confined in the neighborhood of the excited region on the network. Such a feature has been observed in various networks including compact dendrimers [41], star graphs [42], and Apollonian networks [43].

Finally, localization processes may also arise on networks that exhibit random defects. Nevertheless, in this case the influence of the disorder is quite subtle, and different situations occur. On the one hand, the disorder acts as a negative ingredient that completely hinders the excitonic propagation. This feature has been observed, for example, in linear chains [44], discrete rings [45], and binary trees [46]. On the other hand, the disorder behaves as a positive ingredient that enhances the exciton delocalization. For instance, in tree graphs and dendrimers, the presence of a weak disorder generates extended states through fluctuation-enabled resonances between states that initially may appear to be localized [47–49]. Similarly on a Watts-Strogatz network with small-world behavior [50], the efficiency of the excitonic propagation is enhanced when the rewiring probability turns on [51]. Finally, it has been shown that the addition of random bonds to a star graph allows the exciton wave function to spread more [52].

In this context, the aim of the present paper is to characterize how the interplay between the excitonic spectral degeneracy, the exciton-trap coupling, and the presence of disorder affects the trapping process on a complex network. To proceed, following our previous work [53], we consider a network that has been extensively studied in the absence of disorder, i.e., the extended star graph whose central core is occupied by a trap. Organized around a central site, this graph exhibits the local tree symmetry of irregular and complex networks. Without disorder, we have shown that the exciton dynamics is governed by two kinds of eigenstates, namely, many eigenstates associated to highly degenerate real eigenenergies (insensitive to the trap) and three decaying eigenstates characterized by complex energies (sensitive to the trap). As a result, when the exciton is initially located on a peripheral site of the graph, degeneracy-induced localization favors the confinement of an important part of the exciton population in the neighborhood of the excited site. Only a small part of the population is absorbed at the core of the network. Nevertheless, it has been shown that when the size of the network and the exciton-trap coupling are judiciously chosen, the efficiency of the transfer is optimized at ST resulting in the minimization of the absorption time.

All these results being obtained on an extended star graph without disorder, we address here the question whether disorder-induced symmetry breaking modifies the excitonic propagation and affects the trapping process. The present paper is then organized as follows. In Sec. II the disordered extended star graph with a central trap is introduced, and the exciton Hamiltonian is defined. Then the relevant ingredients required for characterizing the dynamics are described. The problem is solved numerically in Sec. III, where a detailed analysis of the excitonic absorption is performed. Special attention is paid for characterizing the way the disorder affects the absorption process. The numerical results are finally discussed and interpreted in Sec. IV.

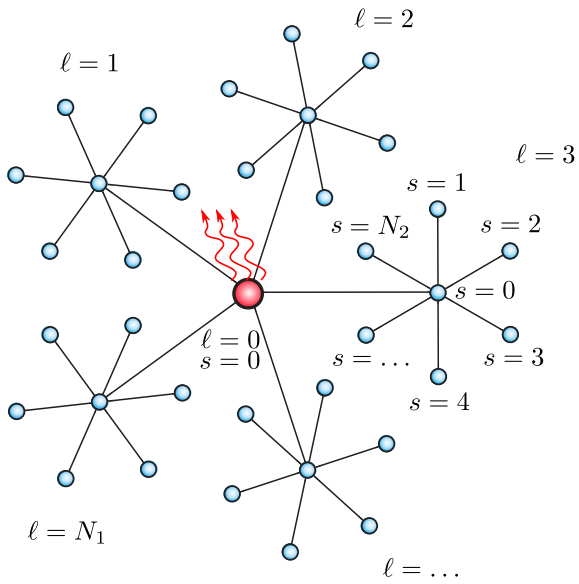

FIG. 1. The extended star graph with an absorbing core.

II. THEORETICAL BACKGROUND

A. Model Hamiltonian

As displayed in Fig. 1, the network we consider is an extended star graph. It defines a two-generation treelike structure formed by N_1 branches that emanate out from a central core. Each branch connects the central core to the central node of N_1 peripheral star graphs. Each peripheral star involves N_2 external branches so that the total number of sites is $N = 1 + N_1 + N_1N_2$. To give a precise description of the sites, we introduce two indexes (ℓ, s): $(\ell = 0, s = 0)$ stands for the central core, $(\ell, s = 0)$, with $\ell = 1, \ldots, N_1$, referring to the central node of the ℓth peripheral star, and (ℓ, s), with $\ell = 1, \ldots, N_1$ and $s = 1, \ldots, N_2$, characterizing the sth peripheral site of the ℓth star.

On this network, the exciton dynamics is modeled as follows. First, we consider that each site (ℓ, s) is occupied by a molecular subunit whose internal dynamics is described by a two-level system with a Bohr frequency $\omega_{\ell,s}$. Let $|\ell, s\rangle$ define the state in which the (ℓ, s)th two-level system occupies its first excited state, all the other two-level systems remaining in their ground state. We will here assume that a trap is located on the central core of the graph. This trap is responsible for an irreversible decay of the exciton according to the decay rate Γ. Within this model, the exciton dynamics is governed by the non-Hermitian effective Hamiltonian [54,55] defined as (within the convention $\hbar = 1$)

$$H = \left(\omega_{0,0} - i\frac{\Gamma}{2}\right)|0,0\rangle\langle 0,0| + \sum_{\ell=1}^{N_1}\sum_{s=0}^{N_2}\omega_{\ell,s}|\ell,s\rangle\langle\ell,s| + \sum_{\ell=1}^{N_1}\Phi(|0,0\rangle\langle\ell,0| + |\ell,0\rangle\langle 0,0|) + \sum_{\ell=1}^{N_1}\sum_{s=1}^{N_2}\Phi(|\ell,0\rangle\langle\ell,s| + |\ell,s\rangle\langle\ell,0|), \quad (1)$$

where Φ is the exciton hopping constant. Note that the convention $\hbar = 1$ will be used throughout this paper. As a result, an energy $\hbar\omega_{\ell,s}$ will be simply denoted $\omega_{\ell,s}$, and any "frequency" will be directly called "energy."

According to the standard Anderson model [56,57], the disorder is introduced by assuming that the site energies $\{\omega_{\ell,s}\}$ are independent random variables uniformly distributed in the interval $[\omega_S - W/2, \omega_S + W/2]$. Here ω_S represents the energy of each site without disorder. Note that, in this paper, ω_S will be taken as the energy reference, i.e., $\omega_S = 0$. The amplitude W represents the strength of the disorder. It defines the variance $W^2/12$ of each site energy.

Due to its non-Hermiticity, the Hamiltonian H exhibits N complex eigenvalues $\hat{\omega}_k = \omega_k - i\gamma_k/2$ (with $k = 1, \ldots, N$) where the real parts ω_k define effective energies, whereas the imaginary parts γ_k represent decay rates (i.e., energy widths). Each eigenvalue is associated to a couple of biorthogonal left or right eigenvectors called $|\tilde{\chi}_k\rangle$ and $|\chi_k\rangle$, respectively. Note that, since H is symmetric, one has the property $\langle \ell, s|\chi_k\rangle = \langle \tilde{\chi}_k|\ell, s\rangle$. Consequently, left and right eigenvectors share a similar weight on each site of the graph: $|\langle \ell, s|\chi_k\rangle|^2 = |\langle \ell, s|\tilde{\chi}_k\rangle|^2$. Also note that in the following, we will consider that each left and right eigenvector is normalized such as $\sum_{\ell,s} |\langle \ell, s|\chi_k\rangle|^2 = \sum_{\ell,s} |\langle \ell, s|\tilde{\chi}_k\rangle|^2 \equiv 1$.

Considering the bi-orthogonality of the eigenvectors, a completeness relation can be introduced $\sum_k |\chi_k\rangle\langle\tilde{\chi}_k|/\langle\tilde{\chi}_k|\chi_k\rangle = \mathbb{1}$, where $\mathbb{1}$ is the identity operator. Using this relation, the excitonic Hamiltonian H can be rewritten in a diagonal form as

$$H = \sum_{k=1}^{N} \hat{\omega}_k \frac{|\chi_k\rangle\langle\tilde{\chi}_k|}{\langle\tilde{\chi}_k|\chi_k\rangle}. \tag{2}$$

B. Quantum dynamics

Following our previous work [53], we consider the particular situation in which the exciton is initially created on the peripheral site ($\ell_0 = 1, s_0 = 1$).

To study the effects of the disorder, we numerically characterize the system properties in the parameter space (Γ, W). To proceed, we first generate a set of N_c disordered configurations. Here the term "configuration" means a network that exhibits a particular landscape of random site energies $\{\omega_{\ell,s}\}$ uniformly distributed over the range $[\omega_S - W/2, \omega_S + W/2]$. The various disordered configurations will be labeled by the specific index (c), with $c = 1, \ldots, N_c$. Then, for each configuration (c), we build and we diagonalize the associated Hamiltonian $H^{(c)}$. One thus obtains the complex eigenenergies $\hat{\omega}_k^{(c)}$ and the eigenstates $|\chi_k^{(c)}\rangle$ (and $|\tilde{\chi}_k^{(c)}\rangle$). From this knowledge, the evolution operator $U^{(c)}(t) \equiv \exp(-iH^{(c)}t)$ is built so that we are able to compute the exciton state $|\Psi^{(c)}(t)\rangle$ at time t as

$$|\Psi^{(c)}(t)\rangle = U^{(c)}(t)|\ell_0, s_0\rangle. \tag{3}$$

Finally, by doing so, we get access to all the information that is required for describing the trapping process. Indeed, let Q denote any relevant quantity such as a site population, an absorption time, or a decay rate, to cite but a few. To study the effect of the disorder on the quantity Q, the knowledge of the exciton properties (eigenenergies, eigenstates, quantum state, and so on) allows us to build the value $Q^{(c)}$ for each configuration (c). One thus finally evaluates the corresponding mean value $\langle Q\rangle$ by performing a statistical average over the N_c disordered configurations.

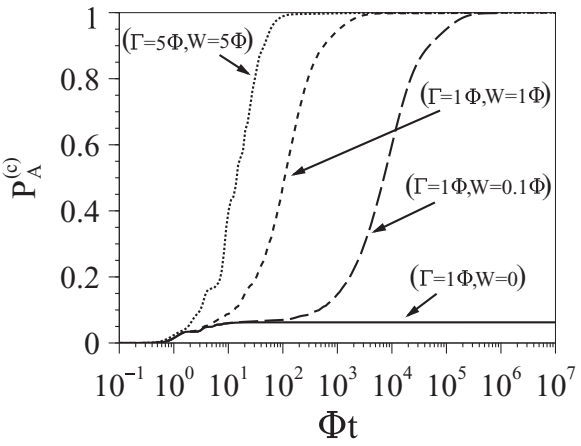

FIG. 2. Time evolution of the absorbed population $P_A^{(c)}(t)$ obtained for particular disordered configurations generated with different values of W and Γ.

This procedure is illustrated in the following section for describing the excitonic absorption process in a disordered extended star graph with fixed parameters $N_1 = N_2 = 4$.

III. NUMERICAL RESULTS

A. Absorption process

To start our numerical analysis, let us show an important property: on an extended star graph, the disorder improves the efficiency of the excitonic absorption. To observe this feature, one introduces the absorbed population $P_A^{(c)}(t)$ defined as

$$P_A^{(c)}(t) = 1 - \sum_{\ell,s} |\langle \ell, s|\Psi^{(c)}(t)\rangle|^2. \tag{4}$$

This quantity is the probability for the exciton to be absorbed by the trap at time t for a given disordered configuration (c). As displayed in Fig. 2, the time evolution of $P_A^{(c)}(t)$ has been computed for particular disordered configurations.

When $W = 0$ (no disorder), the absorbed population increases over a short time $\sim 10\Phi^{-1}$ to reach a maximum value equal to $P_A^{\max} = 6.25 \times 10^{-2}$ indicating that the absorption process is not complete. As the strength of the disorder increases ($W > 0$), a different behavior arises. Indeed, the absorbed population always converges toward unity whatever the disorder. Thus, the presence of defects enhances the absorption process since the whole excitonic population becomes trapped at the core of the graph.

As shown in Fig. 2, the time needed to reach a complete absorption strongly depends on both W and Γ. To characterize this feature, let us introduce the absorption time $\tau^{(c)}$. For each disordered configuration (c), $\tau^{(c)}$ represents the time for which half of the total excitonic population is absorbed:

$$P_A^{(c)}(\tau^{(c)}) = \tfrac{1}{2}. \tag{5}$$

Based on this definition, let us focus on the different time evolutions shown in Fig. 2. For a weak disorder ($\Gamma = 1\Phi, W = 0.1\Phi$), the absorption process exhibits two phases.

During the first phase, a population of about 6.25×10^{-2} is rapidly absorbed over a short time $\sim 10\Phi^{-1}$. Then, over a longer timescale, the absorbed population progressively increases to finally reach unity. The resulting absorption time is $\tau^{(c)} \approx 7 \times 10^3 \Phi^{-1}$. In this situation, the absorption process is complete but not really efficient due to the long time needed to trap the exciton. Nevertheless, this efficiency can be improved if one considers a stronger disorder. With (Γ=1Φ, W=1Φ), the absorbed population directly varies from zero to unity resulting in a shorter absorption time $\tau^{(c)} \approx 100\Phi^{-1}$. A more pronounced enhancement arises when one considers the last configuration with ($\Gamma = 5\Phi, W = 5\Phi$). In this case, the absorbed process is faster, and the absorption time reduces to $\tau^{(c)} \simeq 14\Phi^{-1}$.

All these observations have motivated deeper numerical investigations to better understand the influence of W and Γ on the absorption time $\tau^{(c)}$. To proceed, the mean absorption time $\langle\tau\rangle$ has been numerically estimated. This characteristic time is defined as the geometric mean over the values $\tau^{(c)}$ as

$$\langle\tau\rangle = \exp\left[\frac{1}{N_c}\sum_{c=1}^{N_c}\ln(\tau^{(c)})\right]. \tag{6}$$

The reason why a geometric mean has been introduced instead of the standard arithmetic mean is simple to understand. When carrying out a statistic over the different disordered configurations, it turns out that the distribution of the absorption time exhibits a very long tail. In this context, the use of the arithmetic mean produces irrelevant results since the average value is not representative of the true central tendency of the series. Such an inaccuracy is related to the sensitivity of the arithmetic mean to the few particular values $\tau^{(c)}$ that are very large. To overcome this problem, the solution consists in using another definition for the statistical mean. With long trail distributions, the geometric mean represents a very good option due to the lower sensitivity of this estimator regarding the large singular values of the series.

Based on this definition, the behavior of the mean absorption time $\langle\tau\rangle$ in the parameter space (W, Γ) is shown in Fig. 3(a). Blue curves delimit the isochronal contours of $\langle\tau\rangle$, whereas the black hatched area delimits the zone where $\langle\tau\rangle > 1000\Phi^{-1}$. Figure 3(a) reveals the occurrence of an optimal region where $\langle\tau\rangle$ is strongly reduced. This region is centered around the minimal value of the absorption time $\langle\tau\rangle_{\rm opt} \approx 50\Phi^{-1}$ that arises when the model parameters satisfy $W = W_{\rm opt}$ and $\Gamma = \Gamma_{\rm opt}$ with $W_{\rm opt} \approx \Gamma_{\rm opt} \approx 6\Phi$. When one moves away from this optimal region, $\langle\tau\rangle$ increases. However, such a behavior is not isotropic in the parameter space. Indeed, as illustrated by the isochronal curves, the contours correspond to cigar-shaped isolines more elongated along the Γ direction rather than along the W direction. For instance, along the W direction, the isochronal contour $\langle\tau\rangle = 80\Phi^{-1}$ extends over 10Φ, and it varies from $W = 3\Phi$ to $W = 13\Phi$. By contrast, along the Γ direction, the same isochronal contour extends over 20.5Φ, and it varies from $\Gamma = 1.5\Phi$ to $\Gamma = 22\Phi$. The mean absorption time is then typically twice as sensitive to W as to Γ.

The anisotropic behavior of $\langle\tau\rangle$ hides a more general optimization phenomenon that is highlighted in Fig. 3(b). In this figure, the W dependence of $\langle\tau\rangle$ is displayed for

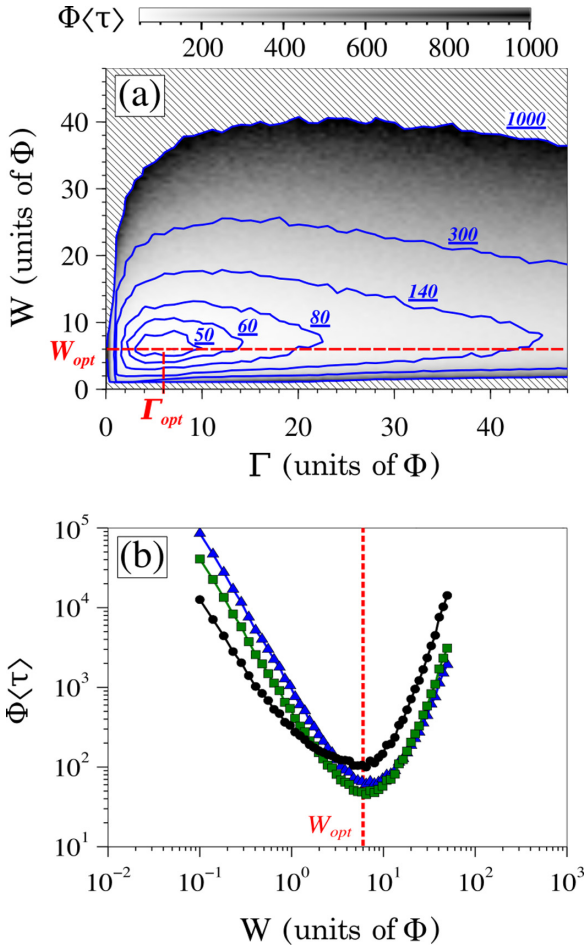

FIG. 3. Behavior of the mean absorption time $\langle\tau\rangle$: (a) depending on the strength of the disorder W and the absorption rate Γ and (b) for three fixed values of the absorption parameter Γ considering W as a free parameter. In panel (b) $\Gamma = 1\Phi$ is represented with black circles, $\Gamma = \Gamma_{\rm opt} = 6\Phi$ with green squares, and $\Gamma = 15\Phi$ with blue triangles. Each value $\langle\tau\rangle$ is the result of a statistic realized over $N_c = 2000$ configurations.

three Γ values. Comparing these three different curves, it clearly appears that, whatever the value of Γ, a minimum of $\langle\tau\rangle$ is always reached when $W \sim W_{\rm opt}$. In the case $\Gamma = 1\Phi$, the minimum mean absorption time is $\langle\tau\rangle \approx 100\Phi^{-1}$. If now the absorption parameter is optimal $\Gamma = \Gamma_{\rm opt} = 6\Phi$, the minimum mean absorption time is superoptimized, and it decreases to $\langle\tau\rangle_{\rm opt} \approx 50\Phi^{-1}$. However, for a larger absorption parameter $\Gamma = 15\Phi$, the mean absorption time admits a larger minimum value that is $\langle\tau\rangle \approx 60\Phi^{-1}$.

B. Study of the active states

To understand the behavior of the mean absorption time, let us now characterize the properties of the system eigenstates. By doing so, we have observed that only a few eigenstates govern the exciton dynamics. Due to their active participation in the trapping process, these particular eigenstates have been renamed "active states."

For describing the active states, we took advantage of the fact that they exhibit a consequent weight $|\langle\ell_0, s_0|\chi_k^{(c)}\rangle|^2$ on

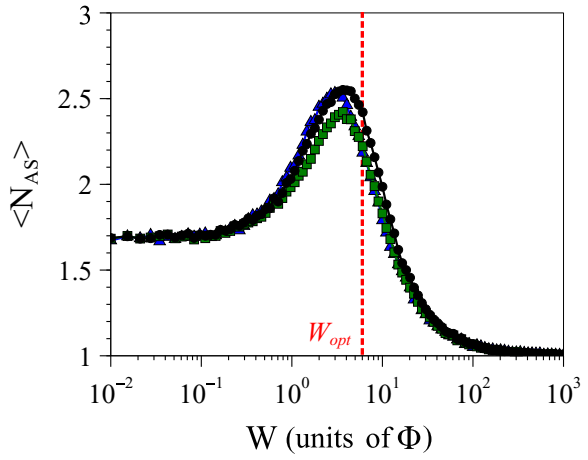

FIG. 4. W dependence of the mean number of active states $\langle N_{\rm AS}\rangle$ for $\Gamma = 1\Phi$ (black circles), $\Gamma = \Gamma_{\rm opt} = 6\Phi$ (green squares), and $\Gamma = 15\Phi$ (blue triangles). Each point of the graph is the result of a statistic realized over $N_c = 2000$ configurations.

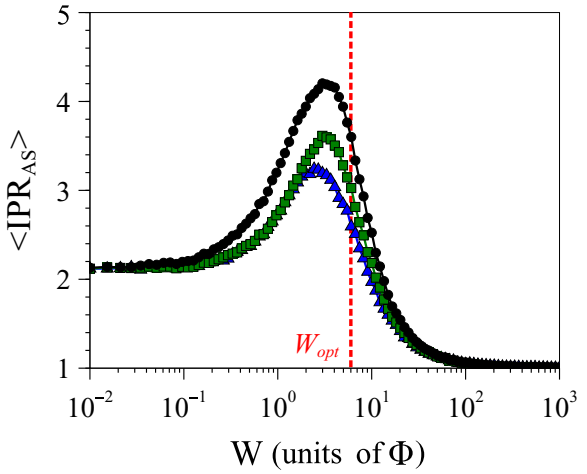

FIG. 5. W dependence of the mean IPR of the active states $\langle {\rm IPR}_{\rm AS}\rangle$ for $\Gamma = 1\Phi$ (black circles), $\Gamma = \Gamma_{\rm opt} = 6\Phi$ (green squares), and $\Gamma = 15\Phi$ (blue triangles). Each point of the graph is the result of a statistic realized over $N_c = 2000$ configurations.

the excited site ($\ell_0 = 1, s_0 = 1$). Based on this property, we have introduced a simple but efficient method to detect the active states. For each configuration (c), an eigenstate $|\chi_k^{(c)}\rangle$ is considered as active only if its weight on the excited site satisfies $|\langle \ell_0, s_0|\chi_k^{(c)}\rangle|^2 \geqslant 10\%$. This choice has been directly inspired by our numerical observations. Indeed, in our study it turns out that each state owning a weight of only a few percent on the excited site does not play a key role in the excitonic absorption and, consequently, behaves as a "nonactive state." In this context, several tests revealed that using a threshold of 10% was a really efficient way to leave apart all these states.

Proceeding with this numerical approach, a complete study of the active states properties has been realized. By doing so, an important thing has been noticed: the active states are always more sensitive to the strength of the disorder W than the absorption rate Γ. This phenomenon clearly reminds us of the behavior of the mean absorption time $\langle\tau\rangle$, as seen previously. Consequently, we will here focus on the effect of the disorder for three cases: $\Gamma = 1\Phi$, $\Gamma = \Gamma_{\rm opt} = 6\Phi$, and $\Gamma = 15\Phi$. In all the following figures, the curves with black circles correspond to results obtained for $\Gamma = 1\Phi$, green squares for $\Gamma = \Gamma_{\rm opt} = 6\Phi$, and blue triangles for $\Gamma = 15\Phi$ (see color figures online).

The first property we consider is the mean number $\langle N_{AS}\rangle$ of active states. It is defined as

$$\langle N_{\rm AS}\rangle = \frac{1}{N_c}\sum_{c=1}^{N_c} N_{\rm AS}^{(c)}, \tag{7}$$

where $N_{\rm AS}^{(c)}$ is the total number of active states detected for the cth disordered configuration.

The W dependence of $\langle N_{\rm AS}\rangle$ is illustrated in Fig. 4. Whatever Γ, a quite similar behavior is adopted as W increases. For small W values, the number of active states is the same: $\langle N_{\rm AS}\rangle \approx 1.7$. Then as W increases, $\langle N_{\rm AS}\rangle$ increases until it reaches a maximum value $\langle N_{\rm AS}\rangle^{\rm max}$. For $\Gamma = 1\Phi$ and $\Gamma = 15\Phi$, $\langle N_{\rm AS}\rangle^{\rm max} \approx 2.6$, whereas for $\Gamma = \Gamma_{\rm opt} = 6\Phi$, $\langle N_{\rm AS}\rangle^{\rm max} \approx 2.4$. Note that this maximization phenomenon always arises in the neighborhood of the optimal disorder $W = W_{\rm opt}$. Then when W exceeds $W_{\rm opt}$ the three curves decrease. They converge toward $\langle N_{\rm AS}\rangle = 1$ within the strong disorder limit $W \gg W_{\rm opt}$.

Let us now consider the mean inverse participation ratio $\langle {\rm IPR}_{\rm AS}\rangle$ of the active states. The inverse participation ratio (IPR) gives a measure of the spatial extension of an eigenstate. For a particular eigenstate $|\chi_k^{(c)}\rangle$, it is defined as

$${\rm IPR}\left(|\chi_k^{(c)}\rangle\right) = \frac{1}{\sum_{\ell,s}\left|\langle \ell, s|\chi_k^{(c)}\rangle\right|^4}. \tag{8}$$

Within this definition, the IPR of an eigenstate localized on one site is equal to 1. By contrast, the IPR of a state uniformly delocalized over the whole graph is equal to N. The mean IPR of the active states $\langle {\rm IPR}_{\rm AS}\rangle$ is written as

$$\langle {\rm IPR}_{\rm AS}\rangle = \frac{1}{N_c}\sum_{c=1}^{N_c}\sum_{k\in AS}\frac{{\rm IPR}\left(|\chi_k^{(c)}\rangle\right)}{N_{\rm AS}^{(c)}}, \tag{9}$$

where $\sum_{k\in AS}$ is a sum over the active states.

The W dependence of $\langle {\rm IPR}_{\rm AS}\rangle$ is shown in Fig. 5. This figure reveals that the evolution of the mean IPR of the active states is quite similar to that of $\langle N_{\rm AS}\rangle$. Indeed, for small disorder W, the three curves start with a same initial value $\langle {\rm IPR}_{\rm AS}\rangle \approx 2.2$. Then when W increases the three curves reach different maximum values $\langle {\rm IPR}_{\rm AS}\rangle^{\rm max}$ that arise in the neighborhood of the optimal disorder $W = W_{\rm opt}$. For $\Gamma = 1\Phi$ the maximum is $\langle {\rm IPR}_{\rm AS}\rangle^{\rm max} \approx 4.2$, whereas for $\Gamma = \Gamma_{\rm opt} = 6\Phi$ it is $\langle {\rm IPR}_{\rm AS}\rangle^{\rm max} \approx 3.6$. The last situation $\Gamma = 15\Phi$ presents a maximum of $\langle {\rm IPR}_{\rm AS}\rangle^{\rm max} \approx 3.2$. After reaching these maxima, the three curves decrease. In the strong disorder limit $W \gg W_{\rm opt}$, they converge toward unity.

To keep on characterizing the spatial extension of the active states, the next property we have estimated is their mean weight $\langle \Pi_{\rm AS}^{\rm core}\rangle$ over the central trap. This quantity is defined as

$$\left\langle \Pi_{\rm AS}^{\rm core}\right\rangle = \frac{1}{N_c}\sum_{c=1}^{N_c}\sum_{k\in{\rm AS}}\frac{\left|\langle 0, 0|\chi_k^{(c)}\rangle\right|^2}{N_{\rm AS}^{(c)}}. \tag{10}$$

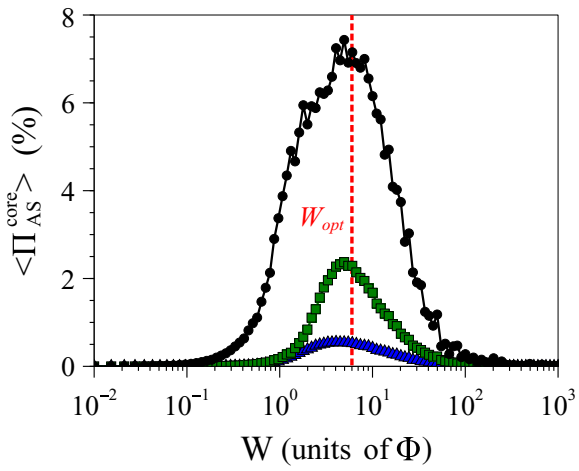

FIG. 6. W dependence of the mean weight on the core site of the active states $\langle \Pi_{AS}^{core} \rangle$ for $\Gamma = 1\Phi$ (black circles), $\Gamma = \Gamma_{opt} = 6\Phi$ (green squares), and $\Gamma = 15\Phi$ (blue triangles). Each point of the graph is the result of a statistic realized over $N_c = 2000$ configurations.

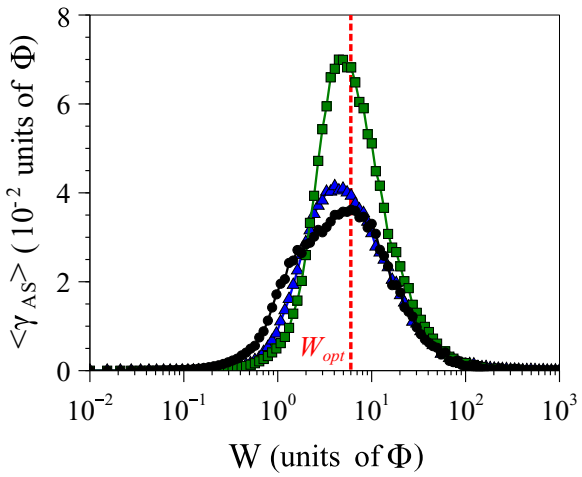

FIG. 7. W dependence of the mean decaying rate of the active states $\langle \gamma_{AS} \rangle$ for $\Gamma = 1\Phi$ (black circles), $\Gamma = \Gamma_{opt} = 6\Phi$ (green squares), and $\Gamma = 15\Phi$ (blue triangles). Each point of the graph is the result of a statistic realized over $N_c = 2000$ configurations.

Figure 6 shows the W dependence of $\langle \Pi_{AS}^{core} \rangle$. Once more, the three curves present a similar progression as W increases. For small disorder, the mean weight of the active states over the core site is very small. For $W = 0.1\Phi$ the amplitude of the three curves ranges in the interval $\langle \Pi_{AS}^{core} \rangle \in [10^{-4}\%, 10^{-2}\%]$. Then as W increases, the curves increase to reach different maxima, all arising in the neighborhood of the optimal disorder $W = W_{opt}$. For $\Gamma = 1\Phi$ the maximum is $\langle \Pi_{AS}^{core} \rangle^{max} \approx 7.2\%$, whereas for $\Gamma = \Gamma_{opt} = 6\Phi$ the value is $\langle \Pi_{AS}^{core} \rangle^{max} \approx 2.4\%$. Finally for $\Gamma = 15\Phi$, one obtains $\langle \Pi_{AS}^{core} \rangle^{max} \approx 0.5\%$. After reaching these maxima, the curves decrease to return to lower values in the strong disorder limit $W \gg W_{opt}$.

Finally, we have investigated the W dependence of the mean decay rate $\langle \gamma_{AS} \rangle$ of the active states. This quantity is defined as

$$\langle \gamma_{AS} \rangle = \frac{1}{N_c} \sum_{c=1}^{N_c} \sum_{k \in AS} \frac{\gamma_k^{(c)}}{N_{AS}^{(c)}}. \tag{11}$$

Figure 7 illustrates the behavior of $\langle \gamma_{AS} \rangle$. Here again, whatever Γ, a quite similar behavior is adopted as W increases. First, for a weak disorder, the mean decay rate is very small. For instance, when $W = 0.1\Phi$ the amplitude of the three curves ranges in the interval $\langle \gamma_{AS} \rangle \in [10^{-5}\Phi, 10^{-4}\Phi]$. Nevertheless, as W increases, the curves progressively increase to reach different maxima all arising in the neighborhood of the optimal disorder $W = W_{opt}$. For $\Gamma = 1\Phi$ the maximum reached is $\langle \gamma_{AS} \rangle^{max} \approx 3.6 \times 10^{-2}\Phi$, whereas for $\Gamma = \Gamma_{opt} = 6\Phi$ the value is $\langle \gamma_{AS} \rangle^{max} \approx 7 \times 10^{-2}\Phi$. Finally for $\Gamma = 15\Phi$ one obtains $\langle \gamma_{AS} \rangle^{max} \approx 4.1 \times 10^{-2}\Phi$. After reaching these maxima, the three curves decrease in the strong disorder limit $W \gg W_{opt}$. For instance, when $W = 100\Phi$ the three curves present a quite similar amplitude $\langle \gamma_{AS} \rangle \sim 10^{-3}\Phi$.

IV. DISCUSSION

When compared with what happens in an ordered network, our results reveal that the disorder drastically improves the excitonic absorption in an extended star graph. Therefore, various properties have been observed.

First, when $W > 0$, it has been shown that the absorption process is complete. Whatever the strength of the disorder, an exciton starting on a peripheral site is always fully trapped at the core site. This feature clearly contrasts with the incomplete trapping process observed in an ordered graph [53].

Then it has been shown that the efficiency of the absorption process strongly depends on the model parameters. Indeed, the behavior of the mean absorption time $\langle \tau \rangle$ in the parameter space (Γ, W) reveals the occurrence of an optimal regime when $W = W_{opt}$ and $\Gamma = \Gamma_{opt}$ with $W_{opt} = \Gamma_{opt} \approx 6\Phi$. In this case, the trapping process is strongly enhanced, and the absorption time $\langle \tau \rangle$ reduces to a minimum approximately equal to $50\Phi^{-1}$. Around this optimal region, the study of the W dependence of $\langle \tau \rangle$ has also revealed the rising of a more general optimization process. Indeed, whatever Γ, a minimization of the absorption time $\langle \tau \rangle$ always occurs in the neighborhood of the optimal disorder $W \sim W_{opt}$.

To understand these behaviors, a study of the active states properties has been realized. Four quantities have been studied: their mean number $\langle N_{AS} \rangle$, their mean IPR $\langle \mathrm{IPR}_{AS} \rangle$, their mean weight on the central trap $\langle \Pi_{AS}^{core} \rangle$, and their mean decay rate $\langle \gamma_{AS} \rangle$. It has been shown that all these quantities reach a maximum value when $W \sim W_{opt}$.

To interpret these features, let us characterize the fundamental ingredients that govern the exciton dynamics, the system eigenstates. Indeed, to be absorbed at the core site (0,0), an exciton initially situated on (ℓ_0, s_0) has to tunnel across the network to reach the trap. According to the fundamental principles of quantum mechanics, this tunneling process, which is encoded in the evolution operator, results from the sum over all the various paths that the exciton can follow to reach the core site at time t. A "path" defines here a transition through an eigenstate $|\chi_k\rangle$ involving specifically its projections on the initial site $\langle \ell_0, s_0 | \chi_k \rangle$ and on the core site $\langle 0, 0 | \chi_k \rangle$. Consequently, the time evolution of the absorption process strongly depends on the eigenstates that actively support the exciton delocalization

to the trap, i.e., the "active states." Depending on whether the graph is ordered or disordered, as well as depending on the strength of the absorption rate Γ, the properties of the active states can change and thus generate various regimes of absorption.

Based on this idea, the scheme of our discussion is simple. As W increases, we will progressively detail the way the disorder modifies the system eigenstates. Let us begin with the case of an ordered graph.

When $W = 0$, the N_1-fold symmetry of the network produces two kinds of eigenstates. On the one hand, $N - 3$ degenerate eigenstates are insensitive to the effect of the trap and exhibit purely real eigenenergies. On the other hand, three nondegenerate decaying states are sensitive to the trap and exhibit complex eigenenergies. Due to their extension over the graph, the three decaying states are the only ones that produce an excitonic tunneling to the core and that participate in the trapping process. However, because of their weak weights on the initial site (ℓ_0, s_0), these eigenstates do not represent real "active states": they govern the dynamics only of a weak part of the total excitonic population. Indeed, as demonstrated in our previous work [53], when an exciton starts from a peripheral site, its dynamics is mainly governed by the highly degenerate eigenstates, which interfere only on the N_1 periphery stars of the network. The resulting interferences produce a localization of the exciton on its initial peripheral star, which therefore hinders the propagation to the trap. As a consequence, the total absorbed population at the core is limited and reaches a maximum of $P_A^{\max} = 1/N_1N_2$. Note that with $N_1 = N_2 = 4$, one obtains the value $P_A^{\max} = 6.25 \times 10^{-2}$ as observed in Fig. 2.

If now a weak disorder $W = 0^+$ perturbs the graph, a different behavior occurs. In this context, the presence of local defects breaks the symmetry of the network. As a result, all the degeneracies are raised, and each eigenstate exhibits a nonzero decay rate. Indeed, due to the disorder, a spatial restructuring of the eigenstates occurs so that each state presents a nonvanishing weight on the core site. As a consequence, each state becomes sensitive to the trap and acquires a finite lifetime. The excitonic population initially located at the periphery of the network can thus entirely transfer to the trap, resulting in a complete absorption process, $P_A^{\max} = 1$.

Nevertheless, in the weak disorder limit, the absorption process remains inefficient. The reason is quite simple to understand. When $W = 0^+$, the eigenstates are weakly perturbed by the disorder so that the graph still keeps the memory of its properties in the absence of disorder. On the one hand, three short-lived eigenstates still remain delocalized over the graph and correspond to the relics of the three decaying states. On the other hand, $N - 3$ long-lived eigenstates are still mainly localized on the peripheral stars of the graph and correspond to the relics of the degenerate states. Due to their very weak (but nonvanishing) weight on the central trap, these states exhibit very small decay rates compared with the three other short-lived states.

In this context, among the $N - 3$ long-lived states are the "active states," i.e., the eigenstates transmitting the main part of the excitonic population to the trap. Due to their long-lived nature, the resulting absorption process varies slowly, and its time evolution exhibits two phases (as observed in Fig. 2). First, over a short timescale, the trapped population increases from zero to $1/N_1N_2$ owing to the action of the three "relic decaying states." Then, due to the influence of the long-lived active states, the absorption process enters in a second phase. Slowly, the active states transmit the remaining excitonic population to the trap. As a result, the absorbed population $P_A(t)$ progressively increases and converges toward unity.

Now, if W increases, the restructuring process induced by the disorder intensifies. As a result, the absorption efficiency is strongly affected, and it exhibits a transition depending on the value of W. First, when W increases the absorption process is enhanced and the time needed to trap the exciton decreases until it reaches a minimum. This minimum occurs in the neighborhood of the optimal value $W = W_{\text{opt}}$. Second, when W exceeds this optimal value, the trapping process progressively loses in efficiency and the absorption time increases.

Understanding the precise origins of this transition is a very difficult task since the latter results from the interplay between different complex mechanisms. However, deeper numerical investigations of the active states have allowed us to gather some key information to interpret this phenomenon. To introduce these features, one will realize a simple thing: tracking the active states for a particular disordered configuration as a function of W. Of course, with this approach we do not pretend to be fundamentally exhaustive. However, based on a simple example, we want here to highlight some typical mechanisms that could explain the existence of the optimal disorder. In this context, Fig. 8 shows the results obtained for a given disordered configuration. On the left part of the figure, the evolution of the eigenenergies is shown (black curves). The red curves represent the eigenenergies of the active states (see color online). On the right part of the figure the spreading of the active states on the extended star graph is represented for (a) a weak disorder, (b) an optimal disorder, and (c) a strong disorder.

In the weak disorder regime, a single active state is present. The corresponding eigenenergy is located at the center of the excitonic spectrum in a place that originally contains many degenerate states when $W = 0$. As a relic degenerate state, this active state remains mainly localized on the peripheral star that initially carries the exciton [see Fig. 8(a)].

When W increases, the restructuring process affecting the eigenstates strengthens, producing a shift of the eigenenergies. When W reaches W_{opt}, the amplitude of the disorder becomes approximately equal to the width of the excitonic spectral band known in the absence of disorder $2\Phi\sqrt{N_1 + N_2} \sim 5.7\Phi$. In this case, the disorder effect becomes strongly nonperturbative. The restructuring process affecting the eigenstates becomes so strong that all the eigenenergies drastically deviate in the spectrum. As a result, avoided crossings appear which indicates the emergence of a new phenomenon: the hybridization of the system eigenstates. Indeed, owing to the presence of the disorder, some resonances may arise between states localized in different regions of the graph. As a consequence, a complex mixing between different relic eigenstates can occur, which generates new paths for the exciton. In this context, as shown in Fig. 8(b), the active states properties evolve: they become more numerous (three states are detected when

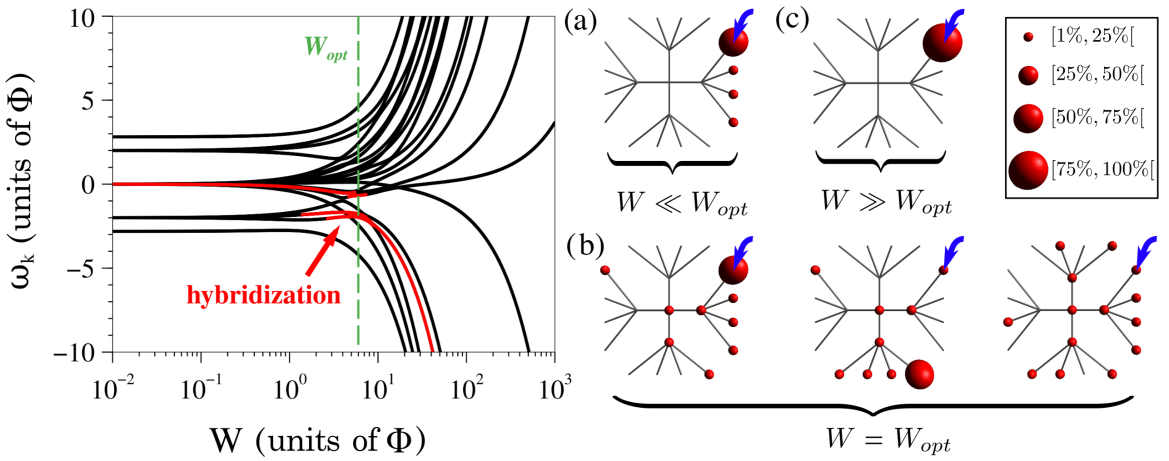

FIG. 8. Tracking of the active states for one particular configuration of disorder for $\Gamma = 1\Phi$. Here the local defects are preserved and scaled with respect to the amplitude W. On the left part of the figure, the graph represents in black the evolution of the real eigenenergies ω_k as a function of W. The red curves indicate the energies of the active states. On the right side an illustration of the spatial extension of the active states is given for three different cases: (a) weak disorder $W \ll W_{\text{opt}}$, (b) optimal disorder $W = W_{\text{opt}}$, and (c) strong disorder $W \gg W_{\text{opt}}$. The size of the balls stands for the weights of the active state on each node whereas the arrow indicates the initial excited site.

$W = W_{\text{opt}}$), and they better spread over the graph. In addition, their weight over the core site is enhanced as well as their widths revealing that they become more sensitive to the trap (not represented here). In this new dynamical context, the excitonic transport changes. The cooperative action of the new active states facilitates the excitonic delocalization from the excited site to the core of the graph. As a result, the absorption time strongly decreases and the trapping process gains in efficiency. At this point, note that all these properties clearly corroborate the maximization of all the quantities $\langle N_{\text{AS}}\rangle$, $\langle \text{IPR}_{\text{AS}}\rangle$, $\langle \Pi_{\text{AS}}^{\text{core}}\rangle$, and $\langle \gamma_{\text{AS}}\rangle$ observed when $W \sim W_{\text{opt}}$.

Now, if W exceeds W_{opt}, the hybridization process progressively vanishes giving rise to another phenomenon: the so-called Anderson localization [56]. Indeed, in the strong disorder limit, the local defects become so important that each eigenstate tends to localize on one particular site. As a consequence, as shown in Fig. 8(c), the number of active states decreases and only one active state subsists. Due to its strong localization on the excited site, this state becomes weakly sensitive to the trap: its weight on the core site and its decay rate vanish when W increases (not represented here). In this context, the exciton remains stuck over a very long time on its initial site, and its propagation from the periphery to the core is hindered. As a result, the absorption time drastically increases, and the trapping process loses its efficiency. Once again, note that these properties corroborate the limit behavior observed when $W \gg W_{\text{opt}}$ for $\langle N_{\text{AS}}\rangle$, $\langle \text{IPR}_{\text{AS}}\rangle$, $\langle \Pi_{\text{AS}}^{\text{core}}\rangle$, and $\langle \gamma_{\text{AS}}\rangle$.

Therefore, within this simple example we have depicted a typical scenario explaining how the eigenstates restructuring induced by the disorder can strongly enhance the absorption process when $W \sim W_{\text{opt}}$. Nevertheless, one last feature still has to be tackled: when $W = W_{\text{opt}}$, the absorption process can be even more optimized if the absorption rate Γ tends to Γ_{opt}. This process gives rise to the occurrence of the optimal region of absorption as presented in Fig. 3.

The emergence of the optimal region of absorption originates in the interplay between two phenomena: the positive restructuring of the eigenstates induced by the disorder and the occurrence of the so-called superradiance transition [36–39]. To better understand this feature, let us consider the optimal disorder $W = W_{\text{opt}}$ as a starting point. In this situation, we know that the restructuring of the eigenstates produces active states exhibiting a maximal weight over the core of the graph (see Fig. 6). As a consequence, these states are in their best predisposition to delocalize the exciton to the trap. Therefore, if Γ starts to increase, the sensitivity of these states to the trap intensifies, which enhances their width (see in Fig. 7 the increasing of $\langle \gamma_{\text{AS}}\rangle^{\text{max}}$ when Γ varies from 1Φ to Γ_{opt}). However, due to the occurrence of a countering phenomenon, this enhancement exhibits a limit. Indeed, as Γ increases, a nonactive state progressively localizes on the trap. As a consequence, all the active states tend to lose their extension over the core of the graph (see in Figs. 6 and 5 the decreasing of $\langle \Pi_{\text{AS}}^{\text{core}}\rangle^{\text{max}}$ and $\langle \text{IPR}_{\text{AS}}^{\text{core}}\rangle^{\text{max}}$ when Γ increases).

When $\Gamma < \Gamma_{\text{opt}}$, this localization is not so significant. The active states then keep improving their interaction with the trap; i.e., their widths increase with Γ. However, when $\Gamma > \Gamma_{\text{opt}}$, the localization process of the nonactive state is so strong that the trap starts to behave as a singular site that almost disconnects from the rest of the graph. In this context, the beneficial interaction of the active states with the trap gets hindered, and a segregation occurs in the decay rates of the eigenstates. On the one hand, the strongly localized nonactive state becomes superradiant: its decay rate keeps on increasing with Γ. On the other hand, the active states become subradiant: their decay rates decrease with Γ (see in Fig. 7 $\langle \gamma_{\text{AS}}\rangle^{\text{max}}$, which diminishes when $\Gamma > \Gamma_{\text{opt}}$). This segregation process that is arising in the neighborhood of Γ_{opt} is the signature of a superradiance transition which gives rise to the optimal region of absorption observed in Fig. 3.

V. CONCLUSION

In this paper, a tight binding model was introduced for studying the dynamics of an exciton moving on a disordered extended star graph whose central site is occupied by a

trap. Quite surprisingly, our work has evidenced the way the disorder improves the absorption process occurring at the core of the graph.

First, in a marked contrast with what happens on an ordered graph, it has been shown that the absorption process is always complete on a disordered graph. The origin of this phenomenon is intimately linked to the symmetry breaking that affects the system. In this context, all the degenerate states that originally hinder the excitonic delocalization become perturbed so that they can participate to the excitonic transport. As a consequence, an exciton starting on a peripheral site can be transferred to the trap, resulting in a complete absorption process.

Second, we have shown the existence of optimal values for both the disorder and the absorption rate. When both parameters are approximately equal to the width of the unperturbed excitonic spectrum, the time needed to trap the exciton strongly reduces. This feature results from the interplay between two complex phenomena. First, when the disorder becomes optimal, a mixing of several relic eigenstates occurs which produces new hybrid states. Owing to their spatial extension, these new hybrid states facilitate the delocalization of the exciton to the trap, which speeds up the trapping. Then a complementary improvement can be done when the absorption rate also reaches its optimal value. In this context, a superradiance transition arises, a transition that enhances the sensitivity of the hybrid eigenstates to the influence of the trap. As a result, the excitonic population reaching the core of the graph is trapped more rapidly, giving rise to a so-called superoptimal absorption process.

Naturally, the study introduced in this paper must be seen as preliminary work that should open complementary investigations. For instance, an interesting question would be to determine how the size of the graph may influence the optimization of the absorption process. In another context, it would also be wise to reconsider this study with a more realistic physical point of view. To do so, considering additional effects of the excitonic environment, such as exciton-phonon interactions and optical recombination, would represent the next logical step of this work.

[1] R. M. Pearlstein, J Chem. Phys. **56**, 2431 (1972).
[2] D. L. Huber, Phys. Rev. B **20**, 2307 (1979).
[3] D. L. Huber, Phys. Rev. B **22**, 1714 (1980).
[4] P. E. Parris, Phys. Rev. Lett. **62**, 1392 (1989).
[5] V. A. Malyshev, A. Rodriguez, and F. Dominguez-Adame, J. Lumin. **81**, 127 (1999).
[6] D. L. Huber, Phys. Rev. B **45**, 8947 (1992).
[7] R. S. Grinyov, A. V. Sorokin, G. Ya. Gural'chuk, S. L. Efimova, I. A. Borovoi, and Y. V. Malyukin, Theor. Exp. Chem. **45**, 58 (2009).
[8] V. M. Kenkre and Y. M. Wong, Phys. Rev. B **23**, 3748 (1981).
[9] J. A. Tuszynski, M. F. Jorgensen, and D. Mobius, Phys. Rev. E **59**, 4374 (1999).
[10] R. P. Hemenger, K. Lakatos-Lindenberg, and R. M. Pearlstein, J. Chem. Phys. **60**, 3271 (1974).
[11] R. E. Fenna and B. W. Matthews, Nature (London) **258**, 573 (1975).
[12] D. Astruc, E. Boisselier, and C. Ornelas, Chem. Rev. **110**, 1857 (2010).
[13] M. B. Plenio and S. F. Huelga, New. J. Phys. **10**, 113019 (2008).
[14] M. Mohseni, P. Rebentrost, S. Lloyd, and A. Aspuru-Guzik, J. Chem. Phys. **129**, 174106 (2008).
[15] J. Wu, F. Liu, Y. Shen, J. Cao, and R. J. Silbey, New. J. Phys. **12**, 105012 (2010).
[16] J. Wu, F. Liu, J. Ma, R. J. Silbey, and J. Cao, J. Chem. Phys. **137**, 174111 (2012).
[17] K. Harigaya, Chem. Phys. Lett. **300**, 33 (1999).
[18] M. A. Martin-Delgado, J. Rodriguez-Laguna, and G. Sierra, Phys. Rev. B **65**, 155116 (2002).
[19] C. Supritz, A. Engelmann, and P. Reineker, J. Lumin. **111**, 367 (2005).
[20] S. Tretiak, V. Chernyak, and S. Mukamel, J. Phys. Chem. B **102**, 3310 (1998).
[21] M. Nakano, M. Takahata, H. Fujita, S. Kiribayashi, and K. Yamaguchi, Chem. Phys. Lett. **323**, 249 (2000).
[22] G. W. Crabtree and N. S. Lewis, Phys. Today **60**(3), 37 (2007).
[23] A. Bar-Haim, J. Klafter, and R. Kopelman, J. Am. Chem. Soc. **119**, 6197 (1997).
[24] M. S. Choi, T. Aida, T. Yamazaki, and I. Yamazaki, Chem. Eur. J. **8**, 2667 (2002).
[25] A. Volta, J. Phys. A: Math. Theor. **42**, 225003 (2009).
[26] Z. Darazs, A. Anishchenko, T. Kiss, A. Blumen, and O. Mulken, Phys. Rev. E **90**, 032113 (2014).
[27] X. P. Xu, Phys. Rev. E **79**, 011117 (2009).
[28] P. L. Krapivsky, J. M. Luck, and K. Mallick, J. Stat. Phys. **154**, 1430 (2014).
[29] E. Agliari, O. Mulken, and A. Blumen, Int. J. Bifurcation Chaos **20**, 271 (2010).
[30] O. Mulken, A. Blumen, T. Amthor, C. Giese, M. Reetz-Lamour, and M. Weidemuller, Phys. Rev. Lett. **99**, 090601 (2007).
[31] O. Mulken and A. Blumen, Physica E **42**, 576 (2010).
[32] O. Mulken and A. Blumen, Phys. Rep. **502**, 37 (2011).
[33] M. Christandl, N. Datta, A. Ekert, and A. J. Landahl, Phys. Rev. Lett. **92**, 187902 (2004).
[34] A. M. Childs, Phys. Rev. Lett. **102**, 180501 (2009).
[35] S. E. Venegas-Andraca, Quantum Inf. Process. **11**, 1015 (2012).
[36] G. L. Celardo, F. Borgonovi, M. Erkli, V. I. Tsifrinovich, and G. P. Berman, J. Phys. Chem.C **116**, 22105 (2012).
[37] G. G. Giusteri, G. L. Celardo, and F. Borgonovi, Phys. Rev. E **93**, 032136 (2016).
[38] Y. Zhang, G. L. Celardo, F. Borgonovi, and L. Kaplan, Phys. Rev. E **95**, 022122 (2017).
[39] G. L. Celardo and L. Kaplan, Phys. Rev. B **79**, 155108 (2009).
[40] O. Mulken and A. Blumen, Phys. Rev. E **73**, 066117 (2006).
[41] O. Mulken, V. Bierbaum, and A. Blumen, J. Chem. Phys. **124**, 124905 (2006).
[42] X. P. Xu, J. Phys. A: Math. Theor. **42**, 115205 (2009).
[43] X. P. Xu, W. Li, and F. Liu, Phys. Rev. E **78**, 052103 (2008).
[44] Y. Yin, D. E. Katsanos, and S. N. Evangelou, Phys. Rev. A **77**, 022302 (2008).
[45] O. Mulken, V. Bierbaum, and A. Blumen, Phys. Rev. E **75**, 031121 (2007).

[46] P. Rebentrost, M. Mohseni, I. Kassal, S. Lloyd, and A. Aspuru-Guzik, New. J. Phys. **11**, 033003 (2009).
[47] M. Aizenman and S. Warzel, J. Eur. Math. Soc. **15**, 1167 (2013).
[48] M. Aizenman and S. Warzel, Phys. Rev. Lett. **106**, 136804 (2011).
[49] V. Pouthier, Phys. Rev. E **90**, 022818 (2014).
[50] D. J. Watts and S. H. Strogatz, Nature (London) **393**, 440 (1998).
[51] B. J. Kim, H. Hong, and M. Y. Choi, Phys. Rev. B **68**, 014304 (2003).
[52] A. Anishchenko, A. Blumen, and O. Mulken, Quantum Inf. Process **11**, 1273 (2012).
[53] S. Yalouz and V. Pouthier, Phys. Rev. E **97**, 022304 (2018).
[54] V. V. Sokolov and V. G. Zelevinsky, Ann. Phys. (NY) **216**, 323 (1992).
[55] V. V. Sokolov and V. G. Zelevinsky, Nucl. Phys. A **504**, 562 (1989).
[56] P. W. Anderson, Phys. Rev. **109**, 1492 (1958).
[57] B. Kramer and A. MacKinnon, Rep. Prog. Phys. **56**, 1469 (1993).